

High-Resolution Molybdenum K-edge X-ray Absorption Spectroscopy analyzed with Time-Dependent Density Functional Theory: Supplementary Information

Frederico A. Lima,^{a,‡§} Ragnar Björnsson,^{a§} Thomas Weyhermüller,^a Perumalreddy Chandrasekaran,^b Pieter Glatzel,^c Frank Neese,^a and Serena DeBeer^{a,d*}

^a Max-Planck-Institut für Chemische Energikonversion, Stiftstrasse 34-36, D- 45470, Mülheim an der Ruhr, Germany Fax: +49 (208) 306 3951; Tel: +49 (208) 306 3605; E-mail: serena.debeer@cec.mpg.de

^b Department of Chemistry and Biochemistry, Lamar University, Beaumont, TX 77710, USA.

^c European Synchrotron Radiation Facility, 6 Rue Jules Horowitz, 38043 Grenoble Cedex, France.

^d Department of Chemistry and Chemical Biology, Cornell University, Ithaca, New York 14853, United States.

‡ Present address: Centro Nacional de Pesquisa em Energia e Materiais, Brazilian Synchrotron Light Laboratory - LNLS, CP 6192, 13084-971 Campinas, SP, Brazil.

List of Figures

S1	Example of the correction of the self-absorption effects in the Mo K-edge HERFD-XAS of compound (1) ($[\text{Mo}^{VI}(\text{O})_3]$). After applying the self-absorption correction the XAS data measured in TFY and transmission modes overlay. The same correction was applied in the HERFD-XAS data.	3
S2	Results of the peak fit procedure for compound (1).	4
S3	Results of the peak fit procedure for compound (2).	4
S4	Results of the peak fit procedure for compound (3).	4
S5	Results of the peak fit procedure for compound (4).	5
S6	Results of the peak fit procedure for compound (5).	5
S7	Results of the peak fit procedure for compound (6).	5
S8	Results of the peak fit procedure for compound (7).	6
S9	Results of the peak fit procedure for compound (8).	6
S10	Correlations between the experimental and calculated Mo K- pre-edge intensity-weighted average energies (<i>left</i>) and intensities (<i>right</i>) obtained using the B3LYP functional and DKH2 relativistic correction.	8
S11	Correlations between the experimental and calculated Mo K- pre-edge intensity-weighted average energies (<i>left</i>) and intensities (<i>right</i>) obtained using the B3LYP functional and ZORA relativistic correction.	8
S12	Correlations between the experimental and calculated Mo K- pre-edge intensity-weighted average energies (<i>left</i>) and intensities (<i>right</i>) obtained using the BP86 functional and DKH2 relativistic correction.	9
S13	Correlations between the experimental and calculated Mo K- pre-edge intensity-weighted average energies (<i>left</i>) and intensities (<i>right</i>) obtained using the BP86 functional and ZORA relativistic correction.	9
S14	Correlations between the experimental and calculated Mo K- pre-edge intensity-weighted average energies (<i>left</i>) and intensities (<i>right</i>) obtained using the BP86 functional and without any relativistic correction.	9
S15	Decomposition of the pre-edge peaks into electric dipole, magnetic dipole and electric quadrupole contributions.	10

Acronyms

XAS	X-ray Absorption Spectroscopy
XANES	X-ray Absorption Near Edge Spectroscopy
EXAFS	Extended X-ray Absorption Fine Structure
HERFD-XAS	High Energy Resolution X-ray Absorption Spectroscopy
TFY	Total Fluorescence Yield
TDDFT	Time-dependent Density Functional Theory
ZORA	Zeroth Order Regular Approximation
DKH2	second order Douglas-Kroll-Hess
COSMO	Conductor-like Screening Model
MLCT	Metal-to-Ligand Charge Transfer
MMCT	Metal-to-Metal Charge Transfer
HF	Hartree-Fock

S1 Experimental Methods

S1.1 HERFD-XAS measurements

The x-ray absorption spectra were collected at the ID26 beamline in the European Synchrotron Radiation Facility. The storage ring was operated in the 7/8 + 1 filling mode, with 200 mA current. The radiation from the ID26 source was monochromatized by a double crystal monochromator using a pair of Si(311) possessing an intrinsic resolution of 0.3×10^{-4} . The x-ray beam size was $200 \times 700 \mu\text{m}$ (V x H) at the sample position. XAS data was also collected in transmission and total fluorescence yield modes concomitant with the high-resolution (HERFD) measurements. A closed-cycle liquid helium cryostat was used to cool down the samples and prevent radiation damage. The temperature at the samples was estimated to be around 40 K. A multi-crystal Johanson-type x-ray spectrometer was used to energy-select the x-ray emission lines and record HERFD-XAS data. It was equipped with five Ge(111) crystals, posed at an Bragg angle of approximately 77.74° . The [999] reflection selected the Mo $K\alpha_1$ emission (~ 17.4 keV). A silicon drift detector was used to record the high-resolution fluorescence (HERFD-XAS), whereas a Si diode was used to record the total fluorescence. The individual contribution of the monochromator and analyzer to the total experimental resolution were determined following the procedure given in Ref.¹. The monochromator resolving power including the vertical divergence of the incident beam is about 25000 (Si (311)), which accounts for less than 1 eV at the Mo K-edge. The intermediate state core-hole lifetime is 4.52 eV, whereas the final state core-hole lifetime is 1.80 eV. Given these parameters, we estimate a total experimental broadening of 3.5 eV with 0.8 eV from the incident beam monochromator and 3.9 eV arising from the X-ray emission spectrometer. Clearly, the analyzer crystals provide the dominant contribution to the instrumental broadening. The energy bandwidth can be readily improved, however, with a loss of detection efficiency. There are efforts underway to reduce the energy bandwidth while maintaining the efficiency. Such efforts will improve the overall energy bandwidth to 2.5 eV in future experiments.

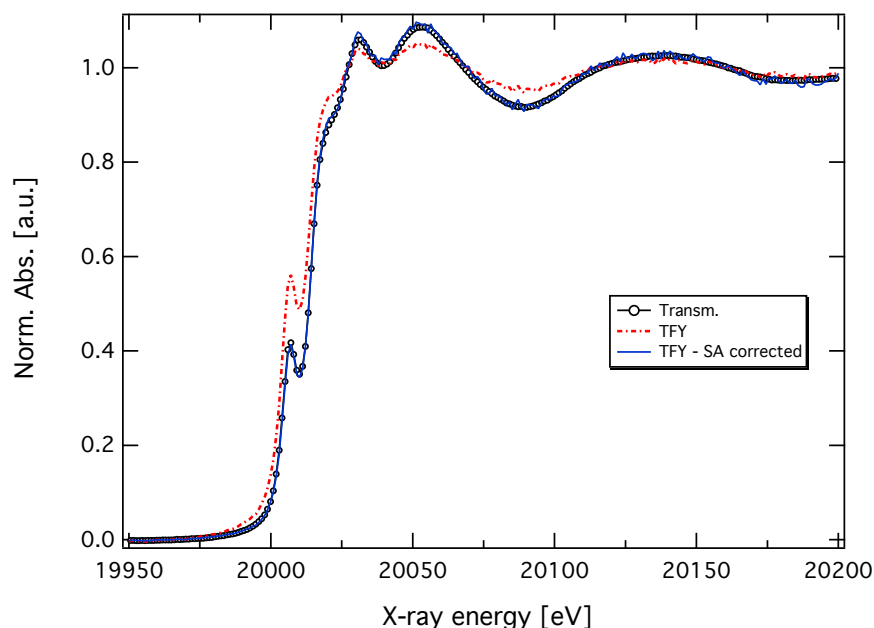


Figure S1 Example of the correction of the self-absorption effects in the Mo K-edge HERFD-XAS of compound (**1**) ($[\text{Mo}^{VI}(\text{O})_3]$). After applying the self-absorption correction the XAS data measured in TFY and transmission modes overlay. The same correction was applied in the HERFD-XAS data.

For each sample several successive spectra were averaged together in order to increase the signal-to-noise ratio. Background subtraction and normalization were performed using the ATHENA package². A first-order polynomial was subtracted from the pre-edge region and third-order from the post-edge region. The atomic background was taken into account by subtracting a spline over the post-edge region using the Autobkg algorithm also implemented in ATHENA.

A comparison of data collected in transmission and total fluorescence yield modes revealed that some samples suffered from self-absorption effects. The XANES data collected in TFY mode was corrected for self-absorption using the “Fluo” algorithm implemented in ATHENA, taking the transmission mode data as reference. The same correction was then applied to the HERFD XAS. An illustration of the self-absorption correction on the XAS data is shown in S1.

S1.2 Fits of the pre-edge peaks

The energy position and areas of the pre-edge features were determined by fitting the peaks using the Blueprint XAS software^{3,4}. The number of peaks in the pre-edge region were estimated by inspection of the second derivative. A set of pseudo-Voigt functions seemed to properly account for features in the pre-edge and the XANES region of the spectrum. The edge was simulated by an actangent function with a step size of one. Between five and seven peaks were needed to reproduce *ca.* 50 eV around the Mo edge region. The results of the peak fit procedure are shown in figures S2, S3, S4, S5, S6, S7, S8 and S9.

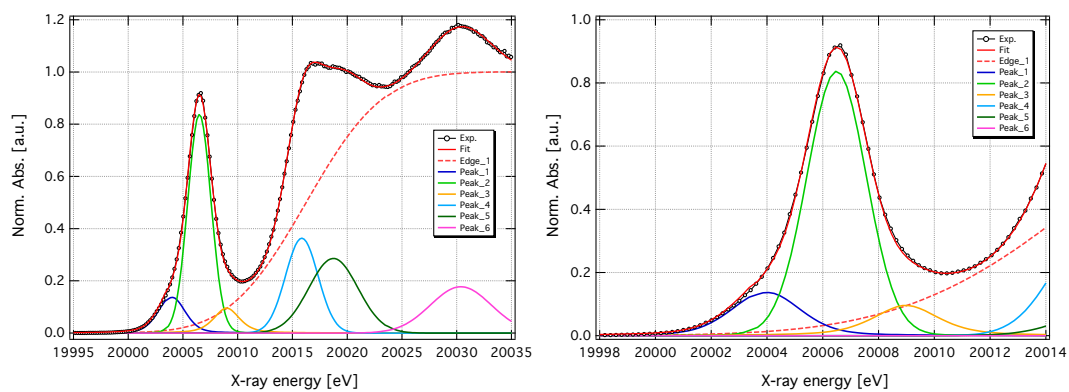


Figure S2 Results of the peak fit procedure for compound (1).

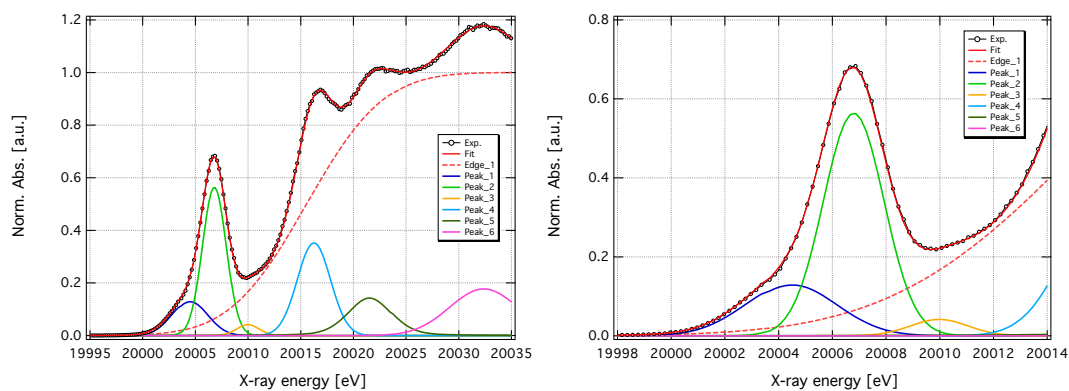


Figure S3 Results of the peak fit procedure for compound (2).

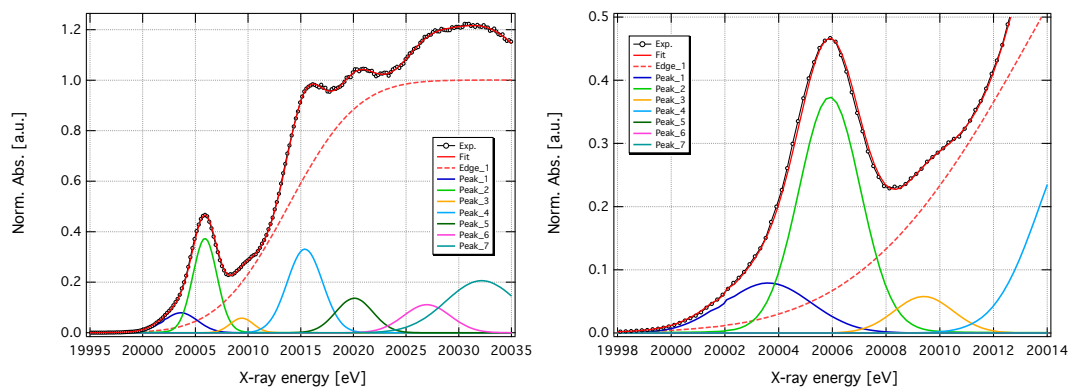


Figure S4 Results of the peak fit procedure for compound (3).

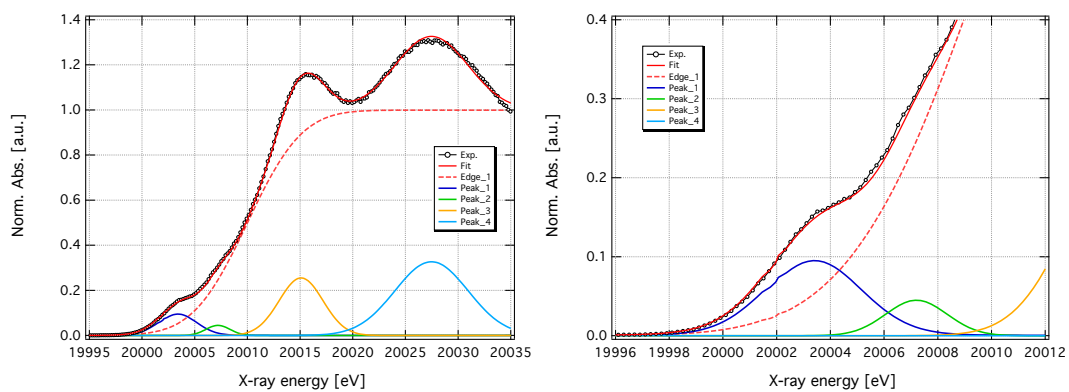


Figure S5 Results of the peak fit procedure for compound (4).

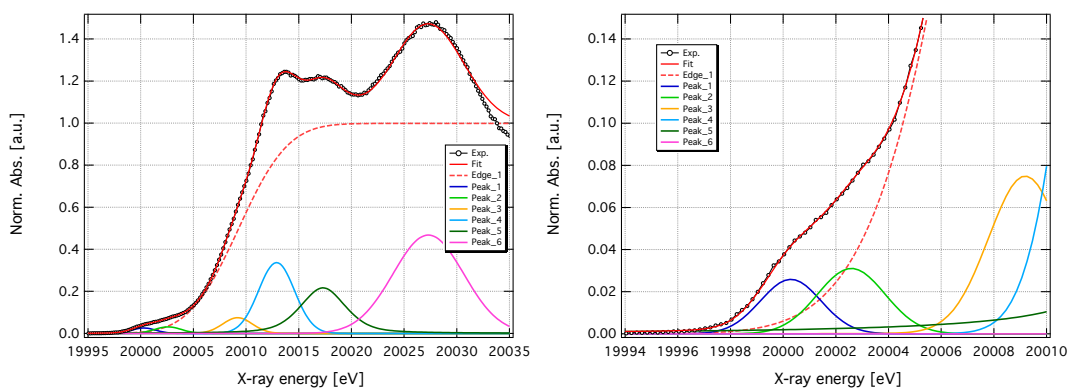


Figure S6 Results of the peak fit procedure for compound (5).

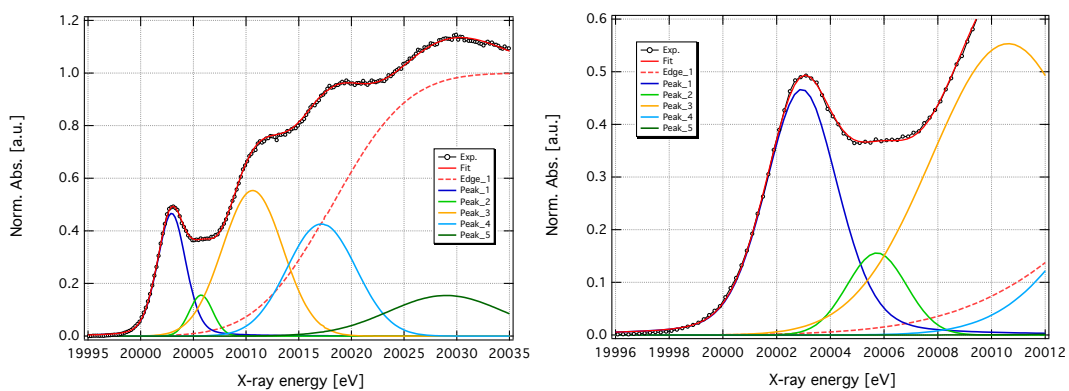


Figure S7 Results of the peak fit procedure for compound (6).

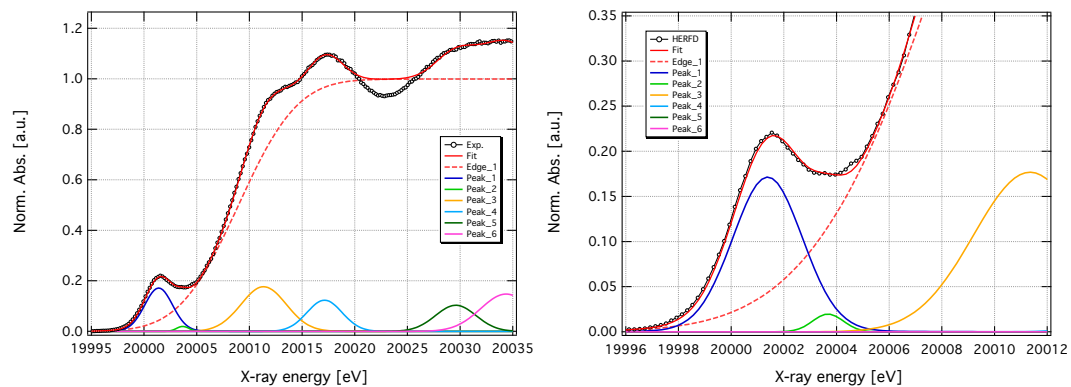


Figure S8 Results of the peak fit procedure for compound (7).

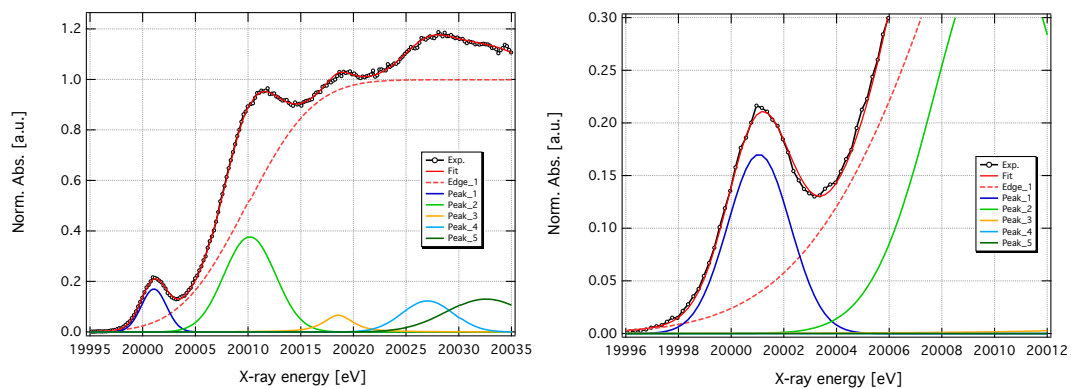


Figure S9 Results of the peak fit procedure for compound (8).

Table S1 Comparison of the calculated energies and intensities of the pre-edge peaks in the Mo K-edge HERFD-XAS for different compounds used in the calibration study

Functional		Compound								Ave. ^a
		(1)	(2)	(3)	(4)	(5)	(6)	(7)	(8)	
BP86 (x-ray)	E	19796.0	19796.1	19795.5	19793.2	19792.7	19791.6	19791.5	19791.4	<i>n.a.</i>
	ΔE	210.0	210.1	209.9	210.2	208.9	211.4	209.9	209.6	210.0 ± 0.7
	Int.	4.953	4.182	3.708	0.485	0.171	2.180	0.840	1.254	<i>n.a.</i>
BP86 (opt)	E	19795.9	19795.9	19795.0	19793.2	19792.64	19791.6	19791.2	19791.4	<i>n.a.</i>
	ΔE	210.1	210.3	210.3	210.2	208.9	211.3	210.3	209.6	210.1 ± 0.7
	Int.	5.052	4.062	2.883	0.520	0.1620	2.203	1.446	1.279	<i>n.a.</i>
B3LYP	E	19853.3	19853.3	19852.3	19850.2	19849.5	19848.8	19849.0	19848.7	<i>n.a.</i>
	ΔE	152.8	153.0	153.1	153.2	152.1	154.1	152.44	152.3	152.9 ± 0.6
	Int.	4.856	4.223	3.070	0.505	0.108	2.1460	1.263	1.190	<i>n.a.</i>
PBE	E	19791.3	19791.3	19792.4	19788.4	19788.0	19787.0	19786.7	19786.8	<i>n.a.</i>
	ΔE	214.8	214.9	212.9	214.9	213.6	215.9	214.7	214.2	214.5 ± 0.9
	Int.	5.001	3.983	2.789	0.473	0.156	2.181	1.209	1.243	<i>n.a.</i>
PBE0	E	19867.3	19867.3	19866.3	19864.2	19863.3	19862.8	19863.1	19862.8	<i>n.a.</i>
	ΔE	138.8	138.9	139.1	139.1	138.3	140.1	138.3	138.2	138.9 ± 0.6
	Int.	4.924	4.324	3.126	0.523	0.091	2.155	1.276	1.212	<i>n.a.</i>
TPSS	E	19815.6	19815.6	19814.7	19812.7	19812.3	19811.2	19810.9	19811.0	<i>n.a.</i>
	ΔE	190.5	190.6	190.7	190.7	189.3	191.8	190.5	190.0	190.5 ± 0.7
	Int.	4.968	4.049	2.864	0.486	0.164	2.186	1.219	1.238	<i>n.a.</i>
TPSSh	E	19843.7	19843.6	19842.7	19840.5	19840.7	19839.2	19839.2	19838.9	<i>n.a.</i>
	ΔE	162.4	162.6	162.7	162.9	160.9	163.7	162.2	162.1	162.4 ± 0.8
	Int.	4.749	3.970	2.878	0.453	0.213	2.046	1.239	1.083	<i>n.a.</i>
revTPSS	E	19816.9	19816.9	19816.0	19814.0	19813.9	19812.5	19812.2	19812.3	<i>n.a.</i>
	ΔE	189.1	189.3	189.4	189.4	187.7	190.5	189.2	188.7	189.2 ± 0.8
	Int.	4.749	3.970	2.878	0.453	0.213	2.046	1.239	1.083	<i>n.a.</i>
revTPSSh	E	19844.8	19844.8	19843.8	19841.7	19840.8	19840.4	19840.3	19840.1	<i>n.a.</i>
	ΔE	161.2	161.4	161.5	161.7	160.8	162.6	161.1	160.9	161.4 ± 0.6
	Int.	5.092	4.262	3.090	0.455	0.069	2.190	1.324	1.163	<i>n.a.</i>
BP86-ZORA	E	20291.5	20291.5	20290.6	20288.7	20288.4	20287.1	20286.7	20287.0	<i>n.a.</i>
	ΔE	-285.4	-285.3	-285.2	-285.3	-286.9	-284.2	-285.3	-286.0	-285.5 ± 0.7
	Int.	4.967	3.988	2.830	0.508	0.193	2.158	1.420	1.248	<i>n.a.</i>
B3LYP-ZORA	E	20349.0	20349.0	20348.0	20345.9	20344.9	20344.5	20344.7	20344.4	<i>n.a.</i>
	ΔE	-342.9	-342.8	-342.6	-342.5	-343.3	-341.6	-343.3	-343.4	-342.8 ± 0.6
	Int.	5.094	4.423	3.222	0.493	0.114	2.249	1.315	1.235	<i>n.a.</i>

^a Ave. refers to the average energy shift.

S2 Correlation plots

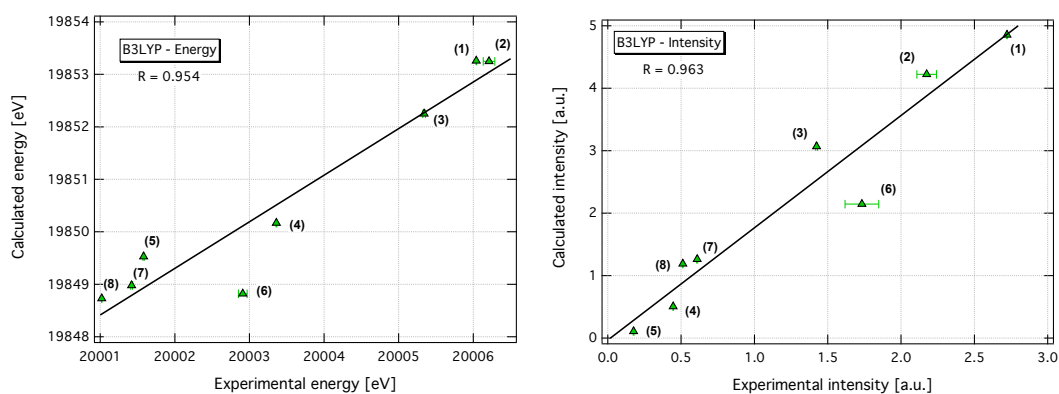


Figure S10 Correlations between the experimental and calculated Mo K- pre-edge intensity-weighted average energies (*left*) and intensities (*right*) obtained using the B3LYP functional and DKH2 relativistic correction.

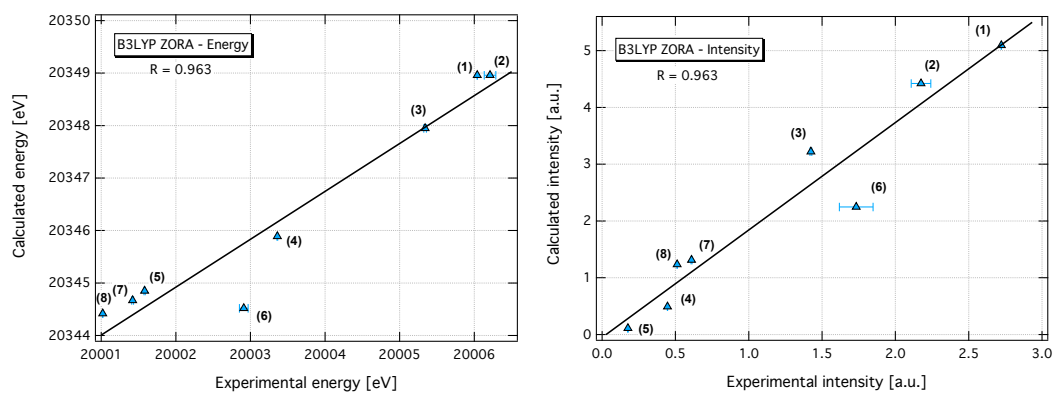


Figure S11 Correlations between the experimental and calculated Mo K- pre-edge intensity-weighted average energies (*left*) and intensities (*right*) obtained using the B3LYP functional and ZORA relativistic correction.

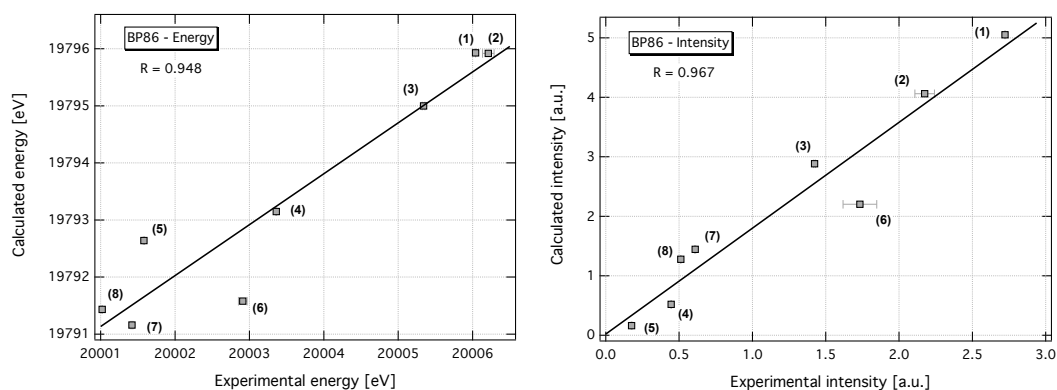


Figure S12 Correlations between the experimental and calculated Mo K- pre-edge intensity-weighted average energies (*left*) and intensities (*right*) obtained using the BP86 functional and DKH2 relativistic correction.

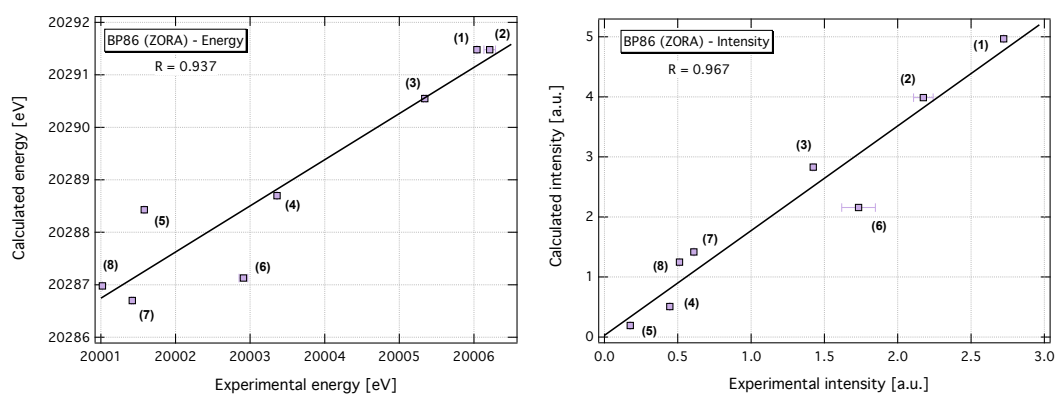


Figure S13 Correlations between the experimental and calculated Mo K- pre-edge intensity-weighted average energies (*left*) and intensities (*right*) obtained using the BP86 functional and ZORA relativistic correction.

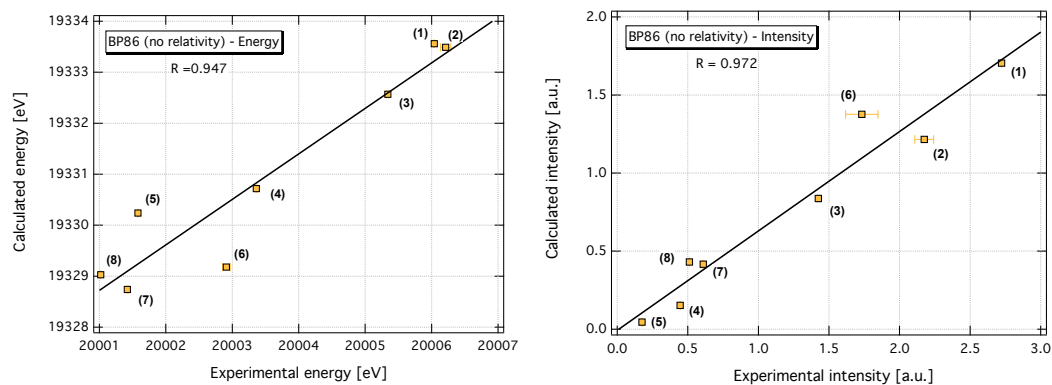


Figure S14 Correlations between the experimental and calculated Mo K- pre-edge intensity-weighted average energies (*left*) and intensities (*right*) obtained using the BP86 functional and without any relativistic correction.

S3 Contribution to the pre-edge

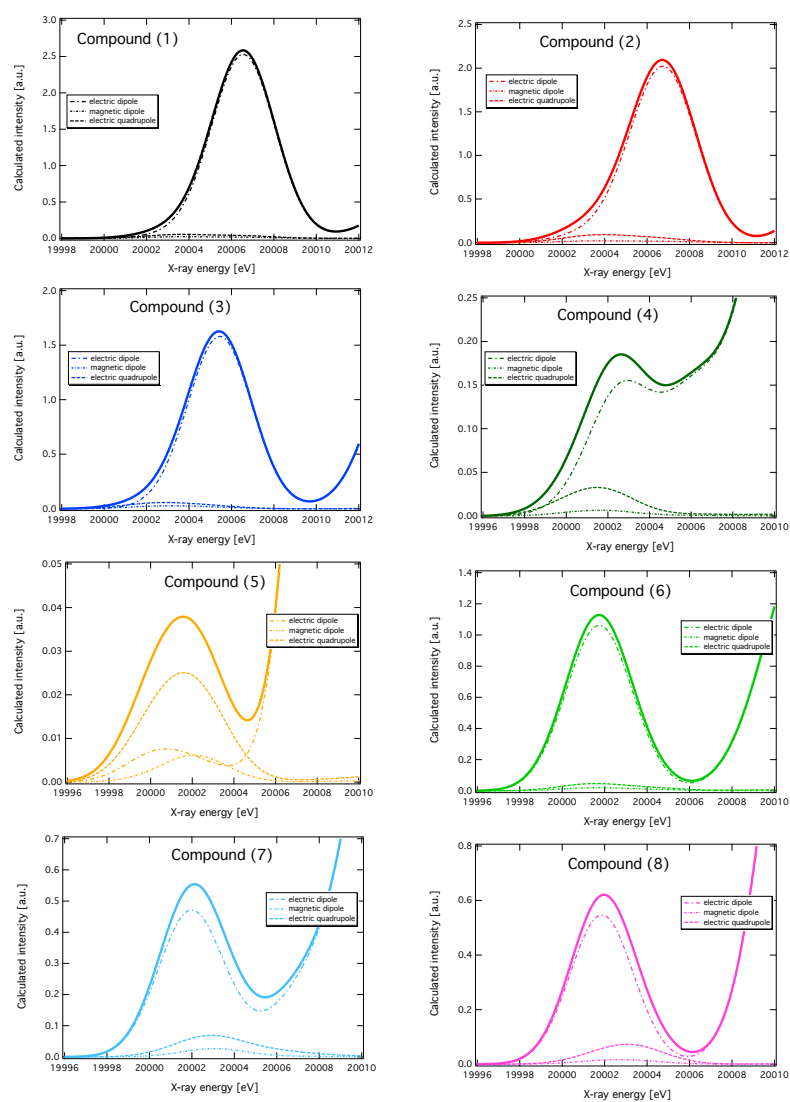


Figure S15 Decomposition of the pre-edge peaks into electric dipole, magnetic dipole and electric quadrupole contributions.

S4 Examples ORCA input files

Geometry optimization

```
!UKS BP86 def2-TZVP def2-TZVP/J DeContractAux ZORA TightSCF vdw10bj
!COSMO Opt xyzfile
%scf
    maxiter 500
end
*xyz charge spin
x y z coordinates
*
```

Spectral calculation

```
!UKS BP86 def2-TZVP def2-TZVP/J DeContractAux DKH2 TightSCF
!COSMO Normalprint xyzfile moread
%method SpecialGridAtoms 42
    SpecialGridIntAcc 7
end
%moinp "geometry-optimization.gbw"
%scf
    maxiter 500
end
%tddft orbwin[0] = 0,0,-1,-1
    orbwin[1] = 0,0,-1,-1
    doquad true
    maxdim 1000
    maxcore 1500
    nroots 60
    triplets false
    end
* xyzfile charge spin geometry-optimization.xyz
```

References

- [1] P. Glatzel, T.-C. Weng, K. Kvashnina, J. Swarbrick, M. Sikora, E. Gallo, N. Smolentsev and R. A. Mori, *J. Electron Spectrosc. Relat. Phenom.*, 2012, DOI: [dx.doi.org/10.1016/j.elspec.2012.09.004](https://doi.org/10.1016/j.elspec.2012.09.004).
- [2] B. Ravel and M. Newville, *J. Synchrotron Radiat.*, 2005, **12**, 537–541.
- [3] M. U. Delgado-Jaime, C. P. Mewis and P. Kennepohl, *J. Synchrotron Radiat.*, 2010, **17**, 132–137.
- [4] M. U. Delgado-Jaime and P. Kennepohl, *J. Synchrotron Radiat.*, 2010, **17**, 119–128.